Chemical Engineering Journal 316 (2017) 988–1003

Contents lists available at ScienceDirect

Chemical Engineering Journal

journal homepage: www.elsevier.com/locate/cej

Investigation of heat transfer in partially filled horizontal drums

Érika Fernanda Rezendes Tada [a,*], Andreas Bück [b], Fernanda Perpétua Casciatori [c], Evangelos Tsotsas [b], João Cláudio Thoméo [a]

[a] Departamento de Engenharia e Tecnologia de Alimentos, Instituto de Biociências, Letras e Ciências Exatas, Universidade Estadual de São Paulo (UNESP), Cristóvão Colombo 2265, Jardim Nazareth, 15054-000 São José do Rio Preto, SP, Brazil
[b] Thermal Process Engineering/NaWiTec, Otto-von-Guericke University, Universitätsplatz 2, 39106 Magdeburg, Germany
[c] Departamento de Engenharia Química (DEQ), Universidade Federal de São Carlos (UFSCar), Rodovia Washington Luiz km 235 (SP-310), 13565-905 São Carlos, SP, Brazil

HIGHLIGHTS

- This paper addresses the study of heat transfer in a particulate system.
- A bed of glass beads placed in a rotating drum is modeled and simulated.
- A one-phase two-dimensional heat transfer model is proposed.
- Parameter optimization is carried out by means of a central composite design.
- The findings are useful for rotating drums bioreactors of solid-state cultivation.

GRAPHICAL ABSTRACT

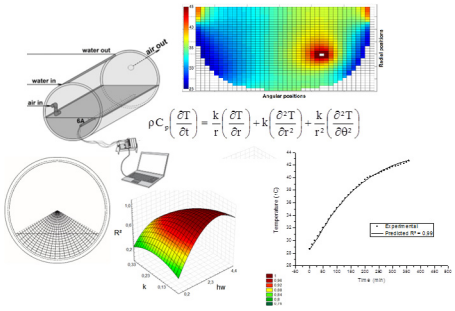

ARTICLE INFO

Article history:
Received 16 September 2016
Received in revised form 22 December 2016
Accepted 27 January 2017
Available online 2 February 2017

Keywords:
Horizontal drum
Heat transfer
Transport parameters
Modelling and simulation

ABSTRACT

The use and the improvement of classical mathematical models for heat transfer in particulate systems can facilitate the industrial large-scale application of rotating drums as bioreactors for solid-state cultivation (SSC). In the current paper, a one-phase two-dimensional heat transfer model is proposed for that radial and angular temperature profiles can be forecasted along time in a horizontal drum, partially filled with glass beads, subjected to intermittent rotation. The most important heat transfer mechanisms were calculated and discussed. Experiments have been carried out in order to provide experimental data of temperature at several radial and angular positions to be compared to the ones predicted by simulation. Three parameters were adjusted to obtain the best fit between simulated and experimental temperature data: h_s, h_w and k (convective heat transfer coefficient bed surface-headspace, convective heat transfer coefficient wall-to-bed and effective thermal conductivity of the bed, respectively). A factorial central composite design (CCD) was used to optimize the search for the best set of parameters, having the determination coefficient as optimization criteria. For the values of the fitted parameters h_s, h_w and k, experimental and predicted temperatures were very close, addressing that the model here can be used as a basic feature for further studies of heat transfer in SSC drum bioreactors and other applications.

1. Introduction

Horizontal drums are widely used as dryers, grinders, mixers, granulators, extractors, calcinators and chemical and biochemical reactors. For solid-state cultivation (SSC), rotating drum represent a flexible bioreactor, in terms of operational conditions or provid-

* Corresponding author.
E-mail address: erikartada@gmail.com (É.F.R. Tada).

http://dx.doi.org/10.1016/j.cej.2017.01.120
1385-8947/

Nomenclature

a	Width of the plate (m)
A_s	Area of the surface of the heated surface
b	Length of the plate (m)
Bi	Biot number (–)
Cp	Specific heat (J °C^{-1} kg^{-1})
f(Ph)	Dimensionless phase transition number (–)
h_s	Convective heat transfer coefficient between the bed surface and the air (W °C^{-1} m^{-2})
h_w	Wall-to-bed convective heat transfer coefficient (W °C^{-1} m^{-2})
i	Number of angular divisions (–)
k	Thermal conductivity (W °C^{-1} m^{-1})
l	Characteristic length for Biot calculations (m)
L	Dimension of the flow (m)
L*	Characteristic length (m)
m	Mass of the bedkg (kg)
Nu	Nusselt number (–)
Pr	Prandtl number (–)
$\dot{q}$	Constant heat flux dissipated by heating element (W m^{-2})
r	Radial position (m)
R	Maximum radius (m)
r*	Half of length of the bed surface (m)
Ra	Rayleigh number (–)
Re	Reynolds number (–)
t	Time (h)
t_c	Time contact (h)
T	Temperature (°C)
$\bar{T}$	Average temperature (°C)
T_a	Air temperature (°C)
T_R	Temperature in the vicinity of the drum wall (°C)
T_s	Temperature at the heated surface (°C)
T_w	Drum wall temperature (°C)
z	Axial position (m)
α	Overall heat transfer coefficient from the heated-surface (W °C^{-1} m^{-2})
θ	Angular position(rad)
β	Internal angle between the bed surface and the maximum radial in relation to geometric center of the circle (rad)
δ	Distance between the maximum height of the bed and the geometric center of the circle (m)
ρ	Density (kg m^{-3})
λ	Maximum height of the bed (m)
ε	Porosity (–)
σ	Dynamic angle of repose (degrees)
φ	Size of each angular division (rad)

Subindices

a	Air
s	Solid material, glass
t	Time-dependence
sp	Property refer to the first layer of particles
bed	Property refer to the penetration heat from the first layer to the bed
so	Property refer to penetration
ws,3	Property from wall to the first layer of particles including radiation

ing several alternatives for control of temperature and moisture content of the reaction medium [1–3].

SSC is defined as the process in which a microorganism is cultivated in a moist particulate substrate, where the water does not exceed the retention capacity of the solid porous matrix [4–7]. SSC has been widely applied to add value to agro-industrial solid by-products. Enzymes, polyols, prebiotic and probiotic products have been obtained from agro industrial wastes, such as pulp and peel (e.g., orange and tangerine), brans (e.g. wheat, rice, soybean), and straws (e.g. wheat, corn, oat) and sugar cane bagasse [8–17]. The concentration and quality of the bioproduct in SSC depends on the capacity of controlling the operational variables close to the optimal conditions for the microbial metabolism.

Two of the most important variables to be controlled in SSC are the temperature and the moisture content of the substrate. The heat generated by the microbial metabolism tends to be accumulated in the cultivation medium, since the effective thermal conductivity of the substrate, usually organic compounds, is low. Usually, the air flow rate through the substrate is low and hot spots can be observed, resulting in moisture migration within the porous medium. The interaction of high temperature and low water concentration negatively affects the microbial metabolism. Therefore, horizontal drums are pointed out to be advantageous for SSC as the drum can be rotated occasionally aiming to homogenize the temperature, and water can be sprinkled over the cultivation medium to replenish the water lost by evaporation. Usually, SSC horizontal drum bioreactors are rotated few times during the cultivation, since the shear stress might harm the hyphaes of filamentous fungi, the most adapted microorganism to this kind of cultivation [18]. Hence, for modelling purposes, these bioreactors can be considered as fixed beds placed in partially filled horizontal cylinders.

Wang et al. [19] presented one-phase models for heat and mass transfers in horizontal drums and validated them using experimental data from a drum filled with milled sweet sorghum stalks, anaerobically fermented by *Saccharomyces cerevisiae* TSH-SC-1. During the experiments, the drum was rotated for 20 min every 5 h. The presented model was able to estimate the temperature at several radial positions along the cultivation, even though only results at the central core were presented, in agreement with the experimental data. However, the heat transfer parameters have not been provided by the authors and little discussion was presented on the heat transfer mechanisms.

Schutyser et al. [20] presented two-phase models for heat and mass transfers in a rotary drum bioreactor. The models were proposed using the discrete elements method, considering the interactions between individual particles. The models were validated with experimental data obtained in the stationary phase of the cultivation of wheat grains by *A. oryzae* CBS 570.64.

Other models for heat transfer available in SSC literature have been proposed for packed beds [21–26], but a specific model has still not been found for a stationary horizontal drum at rest partially filled with particles and aerated through the headspace above the bed. In other fields, several works have been published on heat transfer modelling for rotating drums (see, for instance, [27–30]).

This work proposes a single-phase two-dimensional heat transfer model, where the radial and the angular temperature profiles can be predicted in a bed of inert particles. The model includes the possibility of a heat source in the bed; furthermore the most important heat transfer mechanisms are calculated and discussed. Experiments have been carried out in a drum filled with glass beads and the temperature at several radial and angular positions were measured in order to validate the model. This model will be

the basis for a more general model for heat and mass transfers in a SSC drum bioreactor.

2. Materials and methods

2.1. Experimental setup

The experimental set up is presented in Fig. 1. Air was provided by a radial compressor (1), was filtered to remove oil and particulates (2), had its flow rate controlled by a needle valve coupled to a rotameter (3), and had its temperature controlled in a jacketed tank (4), which was filled with glass beads in order to homogenize the air temperature before entering the jacketed drum (6). A thermostatic bath (5) provided water to the tank (4) and to the drum (6). The inlet and the outlet temperatures of the water in the drum jacket were measured by type T thermocouples and differences lower than 1 °C were observed during the experiments.

The horizontal drum was made of stainless steel, had 31 cm diameter and 74 cm length, and was designed to be used as a solid-state cultivation bioreactor. Through a system of chains and gears, the drum could be rotated at several angular velocities. Two distinct configurations were used: introducing the air through a tube of 3 cm diameter above to the bed surface in parallel to it (Fig. 2a); inserting a cylindrical heating element 1.12 cm diameter within the bed along the longitudinal axis, with no air flow (Fig. 2b). This second configuration was used aiming to simulate a drum bioreactor designed by [31] in which air and steam are introduced in the bioreactor through a perforated tube, place amidst the particles. Such device promotes angular asymmetry, since it is not placed in the central axis of the bed. When using the first configuration, the air entered in the drum 2 cm above the bed surface layer, no matter the drum filling degree.

Twelve type T thermocouples were inserted in the drum in a brass tube of 1.2 cm diameter (6A in Fig. 1). They were positioned in several radial, axial and angular positions, as presented in Fig. 3. The signals from the thermocouples were collected in an A/D acquisition system COMPAQ-DAQ (National, Austin, USA) (7), which was connected to a computer (8), and a LabView v.8. Instruments 5 (National Instruments) routine managed the signals. The thermocouples were disposed in four groups of three thermocouples each: the sensors of the groups 1 and 3 had the same radial and angular positions, but different axial locations; the groups 2 and 4 had the same size, but the sensors were located in different axial and angular locations. The dimensionless axial positions were 0.2, 0.4, 0.6 and 0.8.

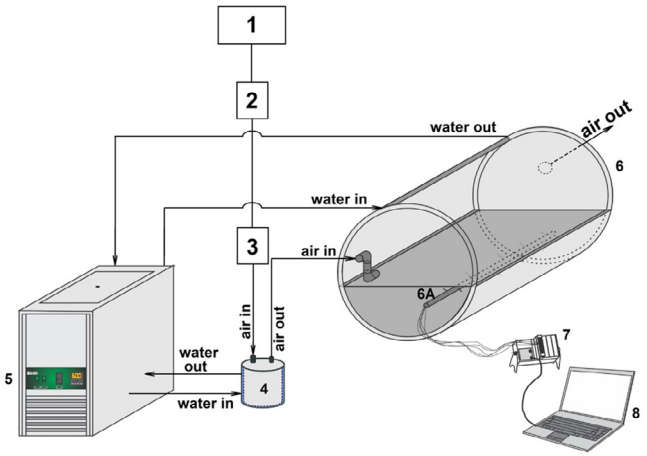

Fig. 1. Experimental setup (1- Radial compressor; 2- filter; 3- rotameter; 4- jacketed recipient filled with glass beads; 5- thermostatic bath; 6- horizontal drum; 6A – Detail of the brass tubes where the thermocouples were inserted in; 7 – Data acquisition system; 8- Computer).

The experiments started flowing water at 45 °C through the drum jacket and either flowing air through the headspace at 45 °C and 5 L/min or powering the heating element at 17.3 W. The steady state was reached after nearly 3 h, which was confirmed by the readings of the thermocouples in the headspace. At this moment, glass beads of 3 mm diameter at 25 °C were loaded in the drum, corresponding to filling degrees 0.2 and 0.4 (27 kg and 37 kg of beads, respectively). The drum was then rotated at 4 rpm during 7 and 9 rotations, for the filling degrees 0.2 and 0.4, respectively, for the bed to achieve the dynamic repose angle, which was visually observed. The drum was halted and henceforward kept static.

2.2. Experimental determination of the convective heat transfer coefficient between the bed surface and the air in the headspace (h_s)

For the experimental determination of the convective heat transfer coefficient h_s between the bed surface and the air flowing in the headspace at 5 L/min, a rectangular electrical resistance 24 cm width and 70 cm length was built and it was longitudinally placed inside the drum. The bottom surface of the plate and the contact points between the plate and the drum wall were thermally insulated using expanded polystyrene in order to have one-dimensional heat flow. The temperature in the thermal insulation below the plate was measured using eight thermocouples. Thermocouples were also installed at six positions on the plate free surface. A CC power supply was connected to the electrical resistance and the heat generated was controlled. A layer of 3 cm of glass beads was placed on the plate free surface. The temperature in the headspace was measured by eight thermocouples placed 10 cm above the bed surface. The position of the plate within the drum followed the filling degrees previously cited. The Newton's Law of Cooling was used to provide h_s.

The experimental value of h_s was compared with values obtained from correlations available in the literature [32–35] for the heat transfer coefficient of Newtonian fluids forcefully flowing in parallel to a flat plate or in free convection.

2.3. Mathematical model

The model proposed for the two adopted configurations (air flowing through the headspace or with a heating element inserted within the bed) is presented in Eq. (1) and derived from one-phase models applied to packed beds. In this equation, the tensor effective thermal conductivity was assumed to be spatially constant and independent of the flow direction:

$$\rho C_p\left(\frac{\partial T}{\partial t}\right) = k\left[\frac{1}{r}\left(\frac{\partial T}{\partial r}\right) + \left(\frac{\partial^2 T}{\partial r^2}\right) + \frac{1}{r^2}\left(\frac{\partial^2 T}{\partial \theta^2}\right) + \frac{\partial^2 T}{\partial z^2}\right] \quad (1)$$

where ρ is the bed apparent density in kg m^{-3}; C_p is the effective heat capacity of the bed in J $°C^{-1}$ kg^{-1}; k is the effective thermal conductivity of the bed in W $°C^{-1}$ m^{-1}; T is the temperature in °C; t is the time in seconds; r, z and θ are the radial, axial and angular coordinate, respectively.

A program in language MATLAB® R2012b, version 2015 (Mathworks Inc., Natick, Massachusetts, USA) was developed for both adopted configurations. The partial differential equations were solved using the finite volume method. This approximation resulted in a set of ordinary differential equations, simultaneously solved by the *ode15s* solver.

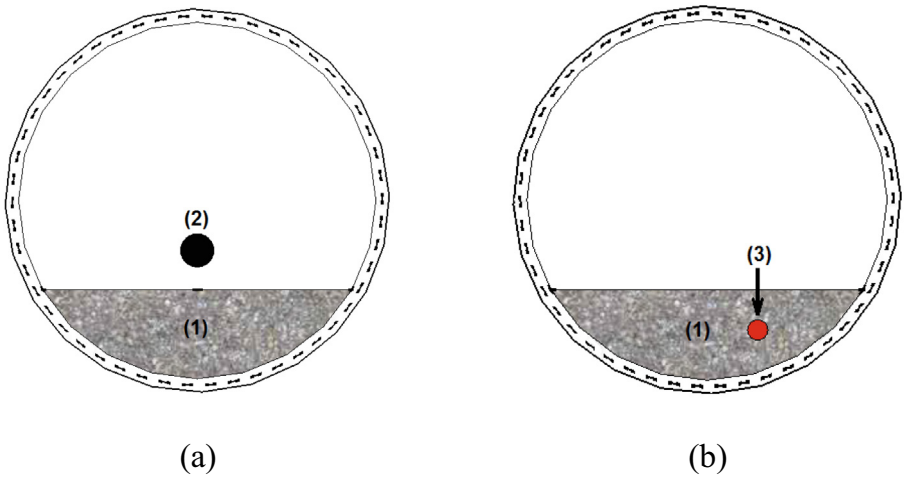

Fig. 2. Frontal view of the horizontal drum. (a) First configuration: air flowing above the bed surface. (b) Second configuration: cylindrical heating element inserted within the bed (1 – Bed of glass beads; 2 – Air inlet; 3 – Cylindrical heating element).

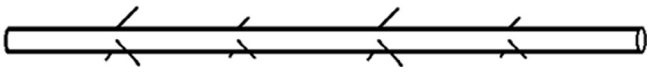

Fig. 3. Distribution of thermocouples on the brass tube for acquisitions of temperature data in the bed.

2.3.1. Configuration with air flowing in the headspace

The geometry of a partially filled cylinder requires the trigonometric relationships to represent the bed surface as the initial position for the integration of Eq. (1), as presented in Fig. 4. The used trigonometric relationships are presented in Eqs. (2)(4).

Admitting θ/2 equal to φ:

$$sen(\varphi) = \frac{\sqrt{2R\lambda - \lambda^2}}{R} \tag{2}$$

$$\beta = \frac{\pi}{2} - \varphi_i \tag{3}$$

The angle φ was divided in *n* increments, with φ_i corresponding to the step of each increment.

$$\varphi_i = \frac{\varphi}{n} \tag{4}$$

For each α_i, a new triangle was considered and its hypotenuse was calculated. The size of R included in the bed for each angle α_i was previously known.

Fig. 5 presents the grid of angular and radial divisions for the numerical solution of Eq. (1) for the filling degree 0.2. The center of the circle is the angular and radial reference and one may observe that there are elements located outside of the bed of particles. The initial radial position depends on the angular position, and the trigonometric relationships previously presented were used to correlate both coordinates depending on the filling degree.

When the configuration with air flowing in the headspace was used, there is angular symmetry, even though the dependence of the temperature with θ is implicit in the dependence of the radial coordinate with the angular coordinate, as follows:

$$\frac{\partial T}{\partial \theta} = \frac{\partial T}{\partial r} \cdot \frac{\partial r}{\partial \theta} \tag{5}$$

As it will be seen in the Results and Discussion section, there is no axial variation of the temperature and the axial heat dispersion term was neglected in Eq. (1), as well as the angular temperature variation, resulting in the following equation:

$$\rho C_p \left(\frac{\partial T}{\partial t}\right) = k\left[\frac{1}{r}\left(\frac{\partial T}{\partial r}\right) + \left(\frac{\partial T}{\partial r^2}\right)\right] \tag{6}$$

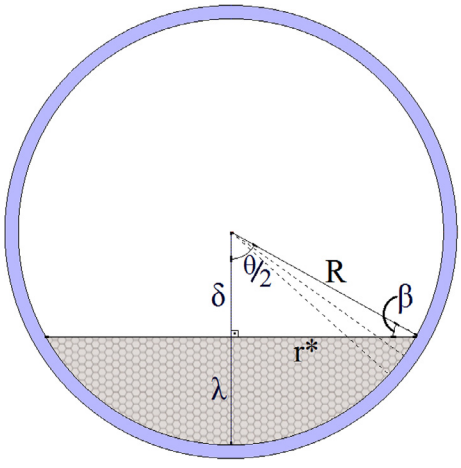

Fig. 4. Variables of interest for determination of trigonometric relationships.

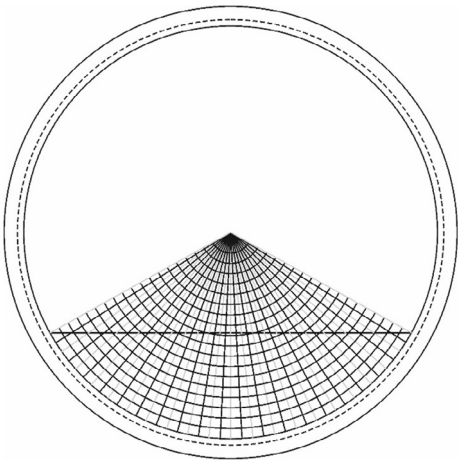

Fig. 5. Front view of the drum for an exemplary filling degree of 0.2. Observe that the reference for the coordinated system is the center of the circle.

Solving the energy balance for a filling degree equal to 1, it represents a full packed bed and the classical solution previously presented in the literature [21,23,25,36–38] are recovered.

To solve the Eq. (6) the initial condition was:

$$t = 0,\ T = T_0 \tag{7}$$

At the bed surface (r = r_i, where T = T_i), a convective boundary condition is used:

$$r = r_i(\theta),\ \frac{\partial T}{\partial r} = -\frac{h_s}{k}(T_a - T_i) \tag{8}$$

where T_a is the temperature of the air in the headspace in °C, assumed to be constant and equal to the temperature of the air inlet.

For the drum wall (r = R) two alternatives were tested: convective heat transfer [36,39] and negligible external resistance:

$$\text{Alternative1}: \quad \frac{\partial T}{\partial r} = -\frac{h_w}{k}(T_w - T_R) \tag{9}$$

$$\text{Alternative2}: \quad T = T_w \tag{10}$$

where h_w is the wall-to-bed convective heat transfer coefficient in W °C^{-1} m^{-2}, T_w is the drum wall temperature in °C, assumed to be equal to the temperature of the water flowing throughout the jacket, and T_R is the temperature in the vicinity of the drum wall, in °C.

2.3.2. Configuration with an immersed tubular heating element within the bed

The electrical tubular resistance introduced angular asymmetry in the system and a two-dimensional model had to be used, as follows:

$$\rho C_p\left(\frac{\partial T}{\partial t}\right) = k\left[\frac{1}{r}\left(\frac{\partial T}{\partial r}\right) + \left(\frac{\partial^2 T}{\partial r^2}\right) + \frac{1}{r^2}\left(\frac{\partial^2 T}{\partial \theta^2}\right)\right] \tag{11}$$

The initial condition and the radial boundary conditions were the same as previously presented, and only the new angular boundary conditions were required. At the connecting points, where the radial and the angular coordinates met, the boundary condition presented by Eq. (8) prevailed.

Three approaches were used to represent the heating element as an additional boundary condition:

Considering constant temperature at the surface (T_s)

$$T = T_s \tag{11a}$$

,

Considering constant heat flux from the element surface ($\dot{q}$):

$$k\frac{\partial T}{\partial \theta} = \dot{q} \tag{11b}$$

Including a heat generation term in the heat balance:

$$\rho C_p \frac{\partial T}{\partial t} = k\left[\frac{1}{r}\left(\frac{\partial T}{\partial r}\right) + \left(\frac{\partial^2 T}{\partial r^2}\right) + \frac{1}{r^2}\left(\frac{\partial^2 T}{\partial \theta^2}\right)\right] + \dot{q} \tag{12}$$

This last alternative is not physically consistent, since not all the bed generates heat, but it was used to verify the distortion in the temperature profile. In Fig. 6 is shown the heating element within the bed, represented by the white circle. The gray circles represented the interfacial region between the bed and the heating element, where the boundary (11a) and (11b) were applied.

2.3.3. Estimation of the parameters

The effective bed parameters ρ, C_p and k were estimated as a weighted average of the properties of the dry air and the properties of the glass using the bed porosity (ε) as weight, as follows:

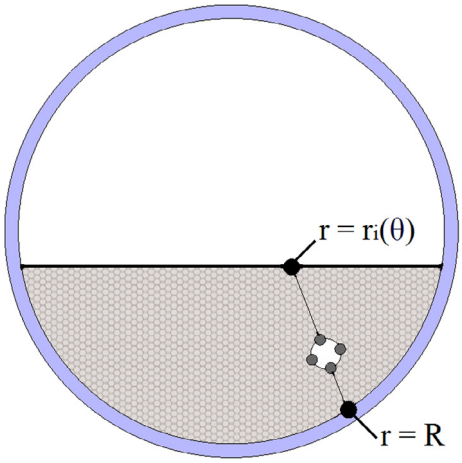

Fig. 6. Spatial distribution of boundary conditions for the configuration with an immersed tubular heating element within the bed.

$$\rho = \rho_s(1-\varepsilon) + \rho_a\varepsilon \tag{13}$$

$$C_p = C_{ps}(1-\varepsilon) + C_{pa}\varepsilon \tag{14}$$

$$k = k_s(1-\varepsilon) + k_a\varepsilon \tag{15}$$

where the subscript *a* corresponds to air and the subscript *s* to the glass beads.

Table 1 presents the values of the air and the glass properties at the film temperature, calculated as the average between the temperature of dry air inlet and initial temperature of the bed.

As previously presented in Section 2.2, h_s was either experimentally obtained or estimated using forced convection or free convection correlations. Therefore, the values of h_s ranged from 0.24 to 4.5 W °C^{-1} m^{-2}.

Three parameters were adjusted to obtain the best fit between calculate and measured temperatures: h_s, h_w and k. To optimize the search for the best set of parameters, a factorial central composite design (CCD) was used, with five central points and eight axial points. The minima and maxima values of the parameters for the CCD are presented in Table 2. The minimum value of k was obtained from Eq. (15) for the minimum value of thermal conductivity of glass beans reported in the cited literature (0.13 W °C^{-1} m^{-1}); the maximum value of k was the one reported by [43]. The minima and maxima values of the convective coefficients (h_s and h_w) were obtained using free convection correlations and forced convection correlations, respectively. The equations corresponding to correlations will be presented in the section 3.2. The determination coefficient (R^2) was used as optimization criteria. The optimized condition was assumed when the set of parameters

Table 1
Physical properties of the dry air and the glass required to estimate the bed properties for the heat transfer simulation.

Symbol	Property	Value	Source
ρ_a	Air density	1.14 kg m^{-3}	[40]
ρ_s	Glass density	2700 kg m^{-3}	
C_{pa}	Air specific heat	1040 J °C^{-1} kg^{-1}	
C_{ps}	Glass specific heat	785–852 J °C^{-1} kg^{-1}	
k_a	Air molecular thermal conductivity	0.02745 W^{-1} °C^{-1} m^{-1}	[41]
k_s	Glass molecular thermal conductivity	0.2–0.44 W^{-1} °C^{-1} m^{-1}	
ε	Average bed porosity	0.38	[42]
σ	Dynamic repose angle	61° (filling degree 0.2) 84° (filling degree 0.4)	This work

Table 2
Range of parameters used to fit the calculated to the experimental temperatures. The parameters were applied to a central composite factorial design to optimize the search of the best fit.

Parameter	Minimum value	Maximum value
k	0.13 W °C^{-1} m^{-1}	0.33 W °C^{-1} m^{-1}
h_w	0.24 W °C^{-1} m^{-2}	4.5 W °C^{-1} m^{-2}
h_s	0.24 W °C^{-1} m^{-2}	4.5 W °C^{-1} m^{-2}

provided the best fit for both filling degrees (0.2 and 0.4). The software Minitab v.16.2.0 (Minitab Inc., State College, USA) was used to generate the surface response and to solve the canonical equations in order to find the optimal conditions. The surface response methodology (RSM) has been chosen to optimize the search of the best set of parameters because it is a relatively simple method that allows the visualization of the prediction space, orienting the choice of the range of parameters in the vicinity of the global maximum based in a relatively small group of runs.

3. Results and discussion

3.1. Longitudinal heat effects

Fig. 7 presents the temperature measured in different axial positions, for the same angular and radial positions, for the filling degree 0.2 and with air flowing throughout the headspace. In this operational condition, the initial temperature of the particles was fixed at 45 °C, while the air inlet temperature, as well as the drum wall temperature, were kept at 25 °C. It is possible to verify that the ending effects were negligible during the whole experiment. Therefore, the use of the term of axial dispersion in the heat balance is indeed unnecessary. At the left hand side of Fig. 6 the angular and radial locations where the temperatures were measured are displayed, a similar representation that will be used henceforth in this paper.

3.2. Experimental determination of the convective heat transfer between the bed surface and the air flowing in the headspace (h_s)

The convective heat transfer coefficient between the bed surface and the air flowing throughout the headspace at 5 L/min was determined for the filling degrees 0.2 and 0.4. Table 3 presents the average temperatures obtained during these experiments, where one may notice little variability among the three replications. The average temperature below the plate, inside of the thermal insulation, was 26.2 ± 0.1 °C at the end of the experiment, for an initial temperature of 25.9 ± 0.3 °C, confirming the hypothesis of one-directional heat flow from the heating element towards the air flowing in the headspace.

The coefficient h_s was also determined using correlations available in the literature for air flowing in parallel to a flat surface and for natural convection [35], which are:

$$Nu_{forced} = \frac{h_s \cdot L}{k_a} = \sqrt{Nu^2_{laminar} + Nu^2_{turbulent}} \quad (16)$$

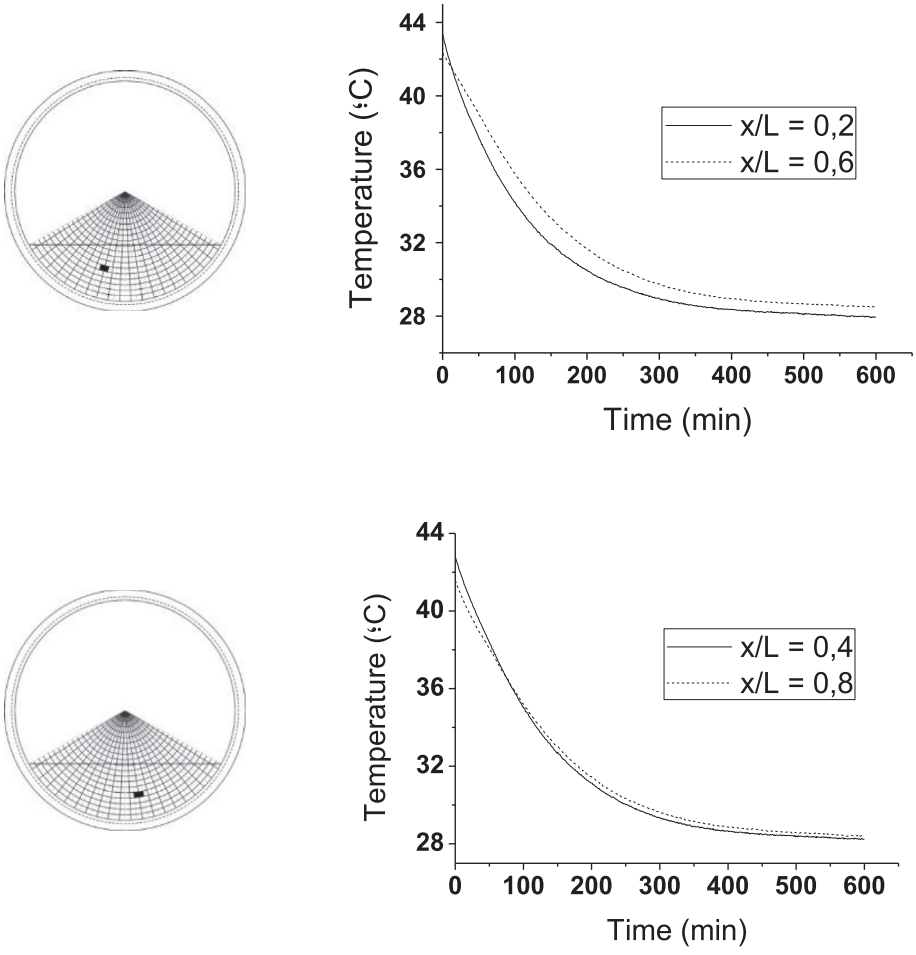

Fig. 7. Temperature obtained in different axial positions for the same angular and radial positions.

Table 3
Measured temperatures for the experimental determination of the heat transfer coefficient between the surface of the particles and the air flowing in the headspace (h_s).

Run	Average temperature on the surface of the resistance (°C)	Average temperature in the headspace (°C)	h_s (W °C^{-1} m^{-2})
1	45.2 ± 0.2	25.1 ± 0.3	4.4 ± 0.1
2	44.9 ± 0.1	25.2 ± 0.4	4.5 ± 0.2
3	45.1 ± 0.1	24.3 ± 0.5	4.3 ± 0.1
Total average	45.0 ± 0.1	24.8 ± 0.4	4.4 ± 0.1

where L is the length of the drum in m, with

$$Nu_{laminar} = 0.664 \mathrm{Re}^{\frac{1}{2}} \mathrm{Pr}^{\frac{1}{2}} \quad (17)$$

$$Nu_{turbulent} = \frac{0.037 \mathrm{Re}^{0.8} Pr}{1 + 2.443 \mathrm{Re}^{-0.1} \left(\mathrm{Pr}^{\frac{2}{3}} - 1 \right)} \quad (18)$$

and

$$Nu_{free} = \frac{h_s \cdot L^*}{k_a} = 0.15 [Ra \cdot f_2(Pr)]^{\frac{1}{5}} \quad (19)$$

with

$$L^* = \frac{a \cdot b}{2(a+b)} \quad (20)$$

where Re, Pr and Ra are, respectively, the Reynolds, the Prandtl and the Rayleigh numbers, dimensionless; and *a* is the width of the plate and *b* is the length of the plate, both in m.

The reference temperature used to determine the physical properties of the air was the film temperature, corresponding to 35 °C.

The velocity required to calculate the Reynolds number in Eqs. (17) and (18) was estimated assuming uniform distribution of the air over the bed surface. The available area for the fluid to flow was 0.17 m^2, resulting in a linear velocity equal to 0.0005 m/s and a Reynolds number equal to 21.3, confirming the assumption of laminar flow in the headspace. The estimated value of h_s calculated using the forced convection equation was 4.54 W °C^{-1} m^{-2} and 0.24 W °C^{-1} m^{-2} for free convection. It must be pointed out that no values have been found in literature for conditions similar to the ones used in this work. Even though the value of h_s obtained by the forced convection equation was very close to the one obtained experimentally, a more extensive study must be done in order to confirm if both situations (air flowing in parallel to a flat surface and air flowing in parallel to a surface of particles in a confined space), are in fact similar, as the particles may introduce local micro turbulence, increasing the heat transfer coefficient values.

3.3. Heat transfer simulation for air flowing in the headspace

The simulation were carried out for the filling degrees 0.2 and 0.4, considering an initial bed temperature of 25 °C, the drum-wall at 45 °C and the air at the entrance of the drum also at 45 °C. Initially, two simulations were performed: assuming negligible the wall-to-bed thermal resistance (constant temperature or first kind boundary condition) and using a wall-to-bed convective (third kind) boundary condition. The mathematical formulation here applied considered angular symmetry [Eq. (6)].

Fig. 8 presents the results for the negligible external resistance for the filling degrees 0.2 and 0.4, corresponding to a maximum bed depth of 8.02 cm and 13.3 cm, respectively. For this simulation, k has been kept at 0.2 W °C^{-1} m^{-1} and h_s at 4.4 W °C^{-1} m^{-2}. The chosen value of k was obtained using Eq. (15), assuming the molecular thermal conductivity of glass as equal to 0.31, the average value between the limits of k_s presented in Table 1. The value of k employed was amidst the usual values found in literature for glass beads (e.g. see Masamune and Smith [43] and Kent and co-workers [45]). Through these simulations, it is possible to verify that the region in the vicinity of the drum-wall assumes the wall temperature shortly after the beginning of the process and that 8 h is enough for thermal equilibrium be achieved.

Fig. 9 presents the simulated temperature profiles for the filling degree 0.4 for times ranging from 3 to 10 h and considering the third kind boundary condition. For these simulations, the parameters k, h_w and h_s have been kept at 0.2 W °C^{-1} m^{-1}, 2.0 W °C^{-1} m^{-2} and 4.4 W °C^{-1} m^{-2}, respectively. The value chosen for h_w corresponding to average value between convective heat transfer coefficients for forcefully convection [Eq. (19)] and free convection [Eq. (16)], both previously calculated. It is possible to notice that the temperature within the bed was lower than those observed for the first kind boundary condition for a same time and that 10 h was not enough to result in thermal equilibrium. The bed temperature near the drum-wall increased slowly along time, showing the importance of the wall-to-bed thermal resistance for the chosen value of h_w. In these conditions, the system tends to thermal equilibrium in about 18 h of process.

The wall effect has been widely studied in literature for heat transfer in packed bed with air flowing perpendicularly to the bed (see, for instance, [36,44]), where the use of a first kind boundary condition always resulted in poor fit between estimated and experimental values of temperatures. Tsotsas and Schlünder [39] claimed that a third kind boundary condition is a reasonable approximation, providing that the region in the vicinity of the wall is small in relation to the tube diameter, as it seems to be the case of the experiments here reported. Even for rotating drums, the use of a first kind boundary condition is not recommended, since Herz and co-workers [29] showed a gradual temperature increase of the particles in contact with the drum-wall, other than a sudden increase. The authors also have shown that the temperature of the particles was always lower than the temperature of the drum-wall and that the thermal equilibrium has not been instantaneously achieved.

3.4. Estimation of parameters for air flowing in the headspace

The parameters h_w and k have been estimated by fitting the temperatures calculated by the model to the temperatures experimentally obtained, assuming h_s as constant (h_s = 4.4 W °C^{-1} m^{-2}, the experimental value). The optimization of the search of the best set of parameters was done using a central composite design (CCD) in order to find the highest coefficient of determination (R^2). Initially, the chosen intervals for h_w and k were wider than the ones presented in Table 2, resulting in a flat response surface in the vicinity of the optimum R^2. Therefore, the intervals were narrowed and the resulting response surface is presented in Fig. 10, where a typical quadratic model represents the surface allowing the search of the maximum R^2. Both parameters showed to be significant, according to the analysis of variance (ANOVA) at 95% of confidence level (see).

The interval proposed for k, from 0.13 to 0.33 W °C^{-1} m^{-1}, included the usually found values of k for stagnant beds (see, for instance, [43,45]). This assumption is valid, since air was not forced to flow through the bed of particles and only free convection takes place within the bed. In respect to the range of h_w, it seems to be under the values often observed in literature for wall-to-bed heat transfer coefficients even for stagnant beds.

The estimated parameters k and h_w that resulted in the highest R^2 were 0.32 W °C^{-1} m^{-1} and 3.0 W °C^{-1} m^{-2}, respectively, for both filling degrees. Figs. 11 and 12 show the calculated and the

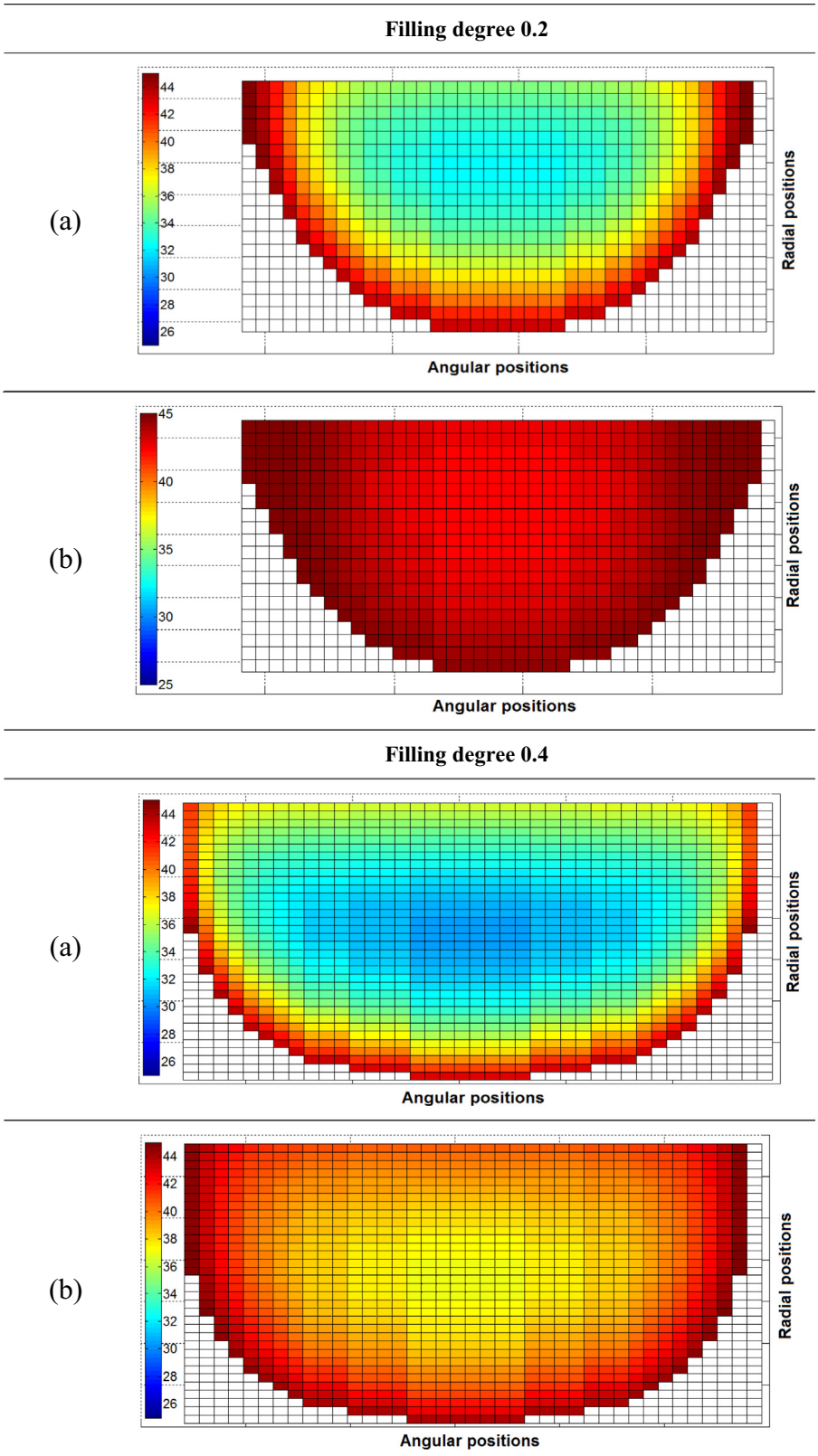

Fig. 8. Simulated temperature profiles using the one-phase model for air flowing throughout the headspace, assuming negligible the external heat transfer resistance, for the filling degrees 0.2 and 0.4 and for (a) 3 h and (b) 8 h of process ($k = 0.2\ W\ °C^{-1}\ m^{-1}$; $h_s = 4.4\ W\ °C^{-1}\ m^{-2}$).

experimental temperatures for angular and radial positions close to the bed surface, central radial position, -agreements for both filling degrees.

To highlight the importance of the thermal resistances in this system, the Biot number could be used, which is defined as:

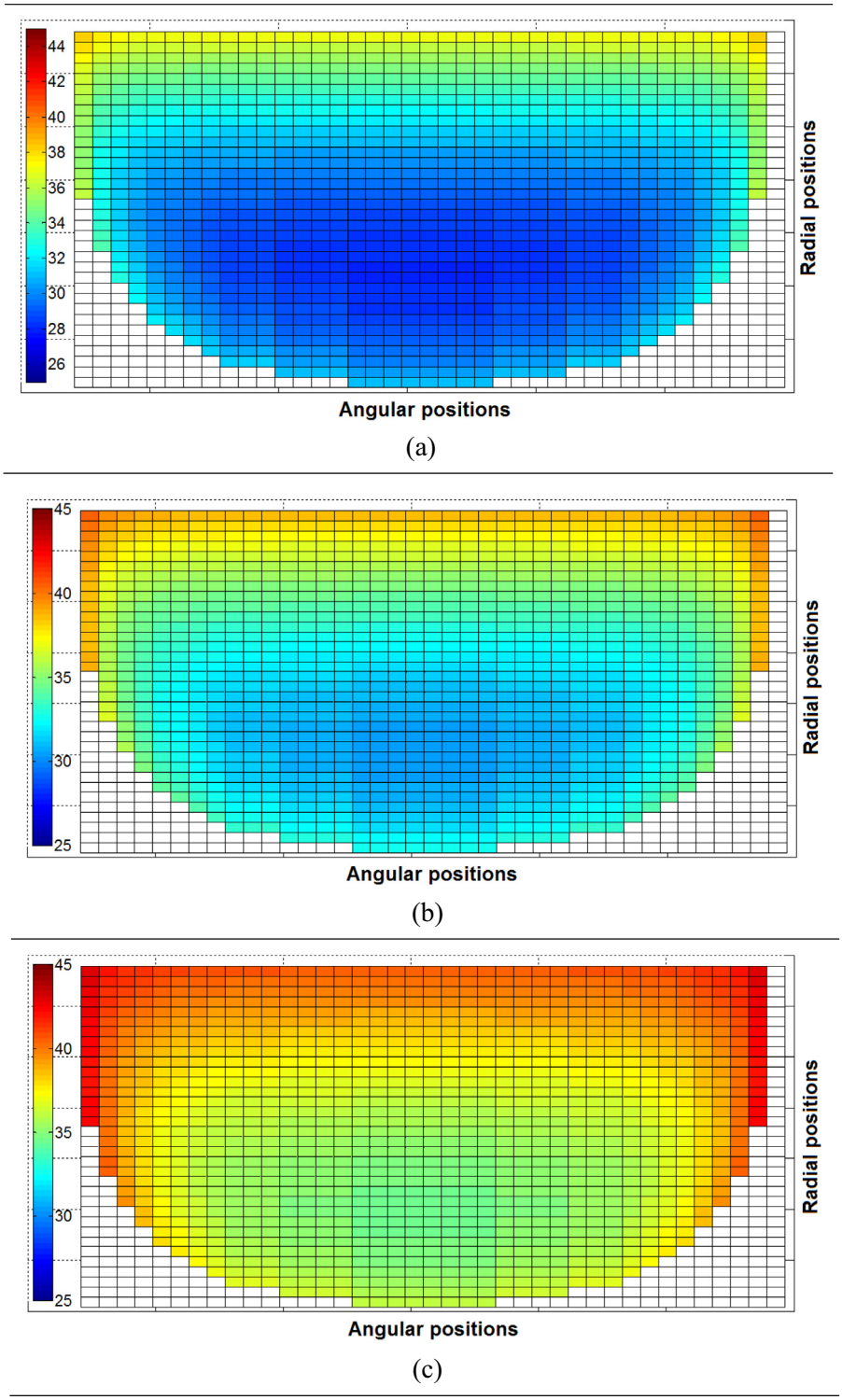

Fig. 9. Temperature profiles simulated using the one-phase model, assuming the significant the external heat transfer resistance, for the filling degrees 0.4 and for (a) 3 h, (b) 6 h and (c) 10 h of process. k = 0.2 W °C^{-1} m^{-1}; h_w = 2.0 W °C^{-1} m^{-2}; h_s = 4.4 W °C^{-1} m^{-2}.

$$Bi = \frac{h_w \cdot \ell}{k} \tag{21}$$

where ℓ is the characteristic length in m, represented by the distance between the wall, r = R, and the point of analysis in the bed, $r_{(\theta)}$, as defined in Eq. (22).

$$\ell = 2 \cdot (R - r_{(\theta)}) \tag{22}$$

Table 4 presents the Biot number for three different positions of the bed (wall, center and surface), with k = 0.32 W °C^{-1} m^{-1} and h_w = 3.0 W °C^{-1} m^{-2} and the temperature increase experimentally obtained between the process startup and after 5 h (ΔT). For the calculation of the Biot number, the heat transferred to the bed of particles from the exterior is considered. From all external sources of heat, the contact thermal resistance, characterized by h_w,

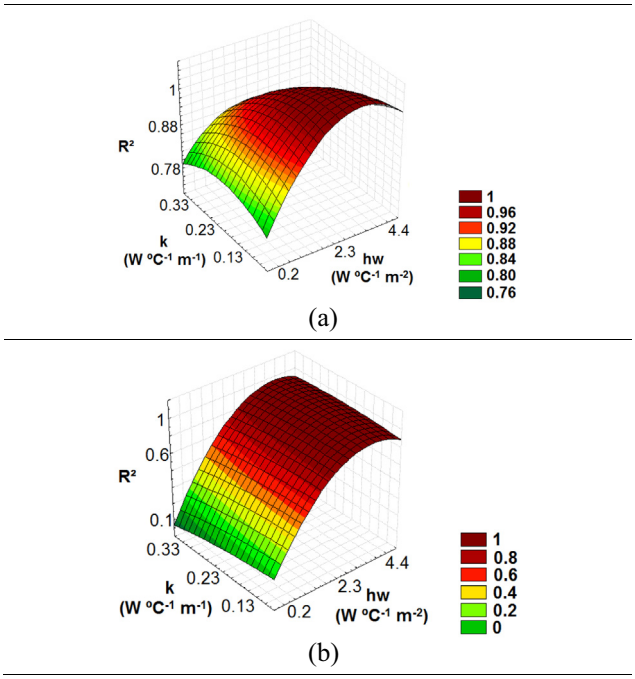

Fig. 10. Response surfaces generated by the CCD used to optimize the search of the best set of h_w and k for air flowing in the headspace, for filling degree 0.4 (a – central position of the bed; b – drum-wall).

dominates the process. Therefore, the definition of Bi here applied uses h_w instead of the traditional convective heat transfer coefficient, here represented by h_s. The hygroscopic nature of the particles has been neglected in this study.

The values of Bi number for the surface and central regions indicated equivalent resistances ($0.1 > Bi > 10$). In the wall region, the value of Biot number under 0.1 implies negligible internal heat resistance justifying the low value of h_w. Therefore, the heat input in the system is governed by the wall-to-bed thermal resistance. This claim is supported by the temperature increase ΔT, since at the near-free-surface position ΔT is lower than near-the-wall position, indicating that the heat transfer between the drum wall and the first layer of particles is more intense than the heat transfer at the bed free surface.

In order to check the range of the estimated overall heat transfer coefficient from the heated wall to the particle bed, we employed the penetration model by Schlünder and Mollekopf [46] and Tsotsas and Schlünder [47], which will be briefly presented. The model is based on an energy balance for the average temperature of a particle bed (with or without mechanical agitation):

$$mc_p \frac{d\bar{T}}{dt} = -\alpha_t (\bar{T} - T_s) A_s \tag{23}$$

where m is the mass of the bed in kg, $\bar{T}$ is the average temperature in °C, α_t is the time-dependent overall heat transfer coefficient from the heated surface (subscript 's') to the interior of the packing, T_s is the temperature of the heated surface in °C and A_s is the area of this surface in m^2. Its value is composed by two contributions: The heat transfer from the surface directly to the first layer of particles in contact with it and the penetration heat transfer from this layer to the interior of the bed. Expressed this concept in terms of thermal resistances:

$$\frac{1}{\alpha_t} = \frac{1}{\alpha_{sp}} + \frac{1}{\alpha_{bed}} \tag{24}$$

As derived by Schlünder and Mollekopf [46], the heat transfer coefficient from a surface at constant temperature to the first layer of particles, α_{sp}, depends on the thermal conductivity of the gas in the voids between particles and the surface, on the particle diameter, and on the modified free path length of the gas molecules. Full details on calculation can be found, elsewhere in [46].

The penetration heat transfer coefficient, α_{bed}, depends mainly on the bed properties and the contact time of particles with the heated surface (t_c) and is given by

$$\alpha_{bed} = \frac{2}{\sqrt{\pi}} \sqrt{\frac{(k/\rho Cp)_{bed}}{t_c}} f(Ph) \tag{25}$$

where for a stagnant dry particle bed, $f(Ph) = 1$. In that case, the contact time t_c of particles in the first layer with the wall corresponds to the process time t. Fig. 13 presents the dependency of α_w with time for a system similar to the one here discussed. The plot depicts the two contributions and the resulting overall heat transfer coefficient. For short process times, like in agitated beds, the wall-particle heat transfer coefficient dominates; for longer times, the penetration coefficient of the bed dominates, reducing the value of α_t. For the process times considered in this study, α_t approaches values in the range of the estimated heat transfer coefficient. Deviations observed with respect to the estimated value from fitting may be due to the fact that the drum is only partially filled, i.e. certain fraction of the material is not in contact with the heated wall. This is not considered in the model of Schlünder and co-workers, which assumes that the material is fully enclosed by the heated surface. Additionally, in the evaluation of the model it was assumed that the particles are completely dry; in the experiment some moisture content may be present, e.g. from the air) which may have significant influence on the bed properties. For further discussion of the model and its applicability, we refer to [46,47].

3.5. Heat transfer simulation for a heating element inserted within the bed

The results for the simulation assuming negligible the wall-to-bed heat resistance, for the configuration in which the heating element is placed within the bed of particles showed the same trends as the ones previously shown for air flowing through the headspace and will not be discussed.

Fig. 14 presents the results for the simulation considering a third kind boundary condition at the drum-wall for the filling degree 0.4 for 10 h of simulation, considering the three alternatives of representing the influence of the heating element in the heat balance:

(a) as a first kind boundary condition;
(b) as a second kind boundary condition (constant heat flux);
(c) as a heat generation term included in the heat balance.

In these simulations, the two-dimensional model was applied and k has been fixed at 0.13 and 0.33 W °C^{-1} m^{-1}, h_w at 2.0 W °C^{-1} m^{-2}, and h_s at 0.24 W °C^{-1} m^{-2}, the value calculated using a correlation for free convection [35].

When the options (a) and (b) were used, the asymmetry of the angular temperature profile is evident; nevertheless, for the option (c) the temperature profile is similar to the one observed for the configuration with air flowing throughout the headspace, indicating that the rate of heat dissipated by the resistance (17.3 W) is not high enough to distort the angular temperature profile.

If the temperature is assumed constant at the interface heated element-bed [option (a)], the temperature in the vicinity of the

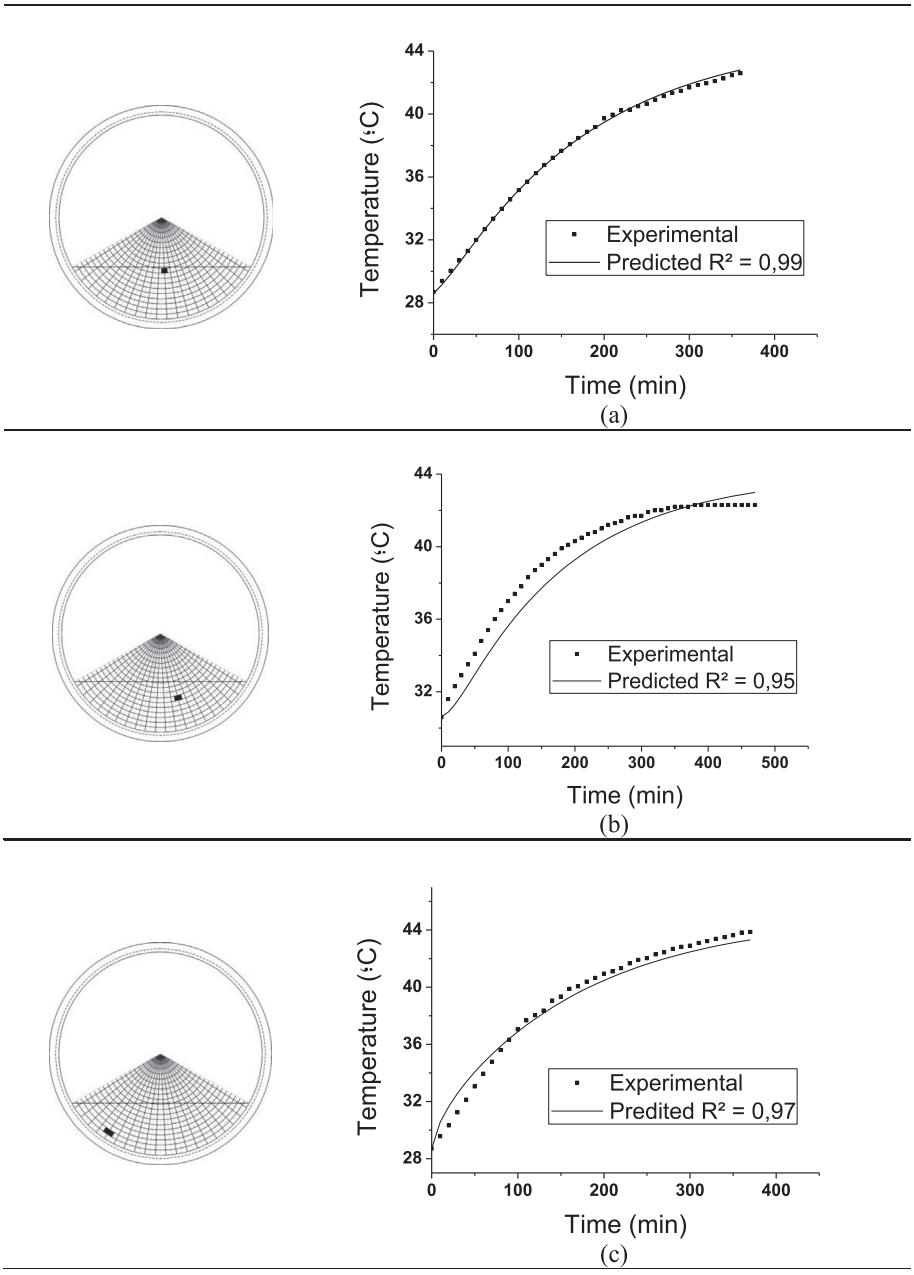

Fig. 11. Temperature profiles calculated by the one-dimensional model for the best set of parameters ($k = 0.32\ W\ °C^{-1}\ m^{-1}$; $h_w = 3.0\ W\ °C^{-1}\ m^{-2}$; $h_s = 4.4\ W\ °C^{-1}\ m^{-2}$) and experimental values obtained for the filling degrees 0.2 at the region near the bed topmost surface (a), in the central core (b), and in the vicinity of the drum-wall (c).

element reaches 45 °C after 10 h of simulation. On the other hand, if a constant heat flux was used [option (b)], the temperature in the same region achieves 75 °C for $k = 0.13\ W\ °C^{-1}\ m^{-1}$ and 55 °C for $k = 0.33\ W\ °C^{-1}\ m^{-1}$, indicating the strong influence of k in the heat removal in terms of range of temperatures, but not in relation to spatial temperature profiles. After 10 h of simulation, the region neighbor to the drum wall (assumed as 3 d_p) assumed temperatures close to the wall temperature (45 °C), a different result from the one observed for air flowing through the headspace, in which the temperature increase was milder. Probably, the reduction of h_s, in the configuration with the heating element, reduced the heat removal by the bed surface, and the heat introduced in the bed by the drum-wall is poorly removed throughout the bed of particles with low effective thermal conductivity.

3.6. Estimation of parameters for a heating element inserted within the bed

Initially, the experimental temperature measured at a region near the bed surface for the filling degree 0.4 was compared with the simulated temperature considering the three already stated options of representing the heating element in the heat balance. In this simulation, the parameters k, h_w and h_s have been kept as $0.32\ W\ °C^{-1}\ m^{-1}$, $3.0\ W\ °C^{-1}\ m^{-2}$ and $0.24\ W\ °C^{-1}\ m^{-2}$, respectively. The temperature profile obtained when a term of heat generation was included in the heat balance [option (c), Eq. (12)] was similar to the one obtained with the one-dimensional model; therefore, this option was not considered for further analysis. For the option (b), the trend of increase of the temperature along time

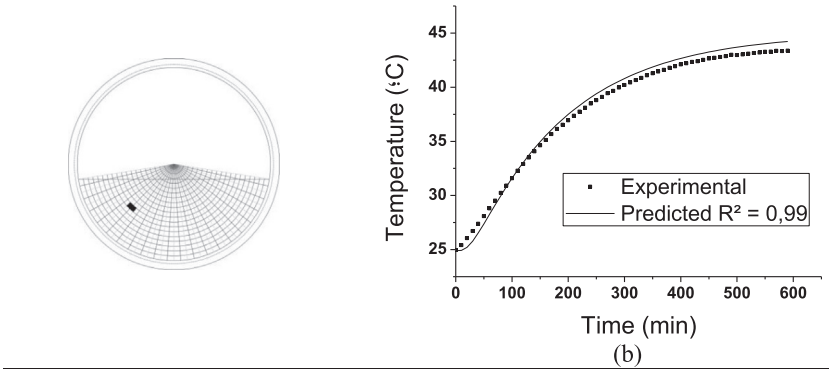

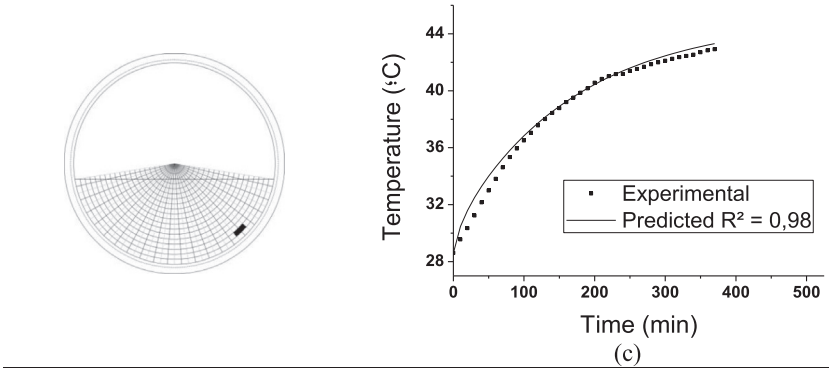

Fig. 12. Temperature profiles calculated by the one-dimensional model for the best set of parameters ($k = 0.32\ W\ °C^{-1}\ m^{-1}$; $h_w = 3.0\ W\ °C^{-1}\ m^{-2}$; $h_s = 4.4\ W\ °C^{-1}\ m^{-2}$) and experimental values obtained for the filling degrees 0.4 in the central core (b) and in the vicinity of the drum-wall (c).

Table 4
Biot number in distributed positions in the bed ($k = 0.32\ W\ °C^{-1}\ m^{-1}$ and $h_w = 3.0\ W\ °C^{-1}\ m^{-2}$) and the experimental temperature variation from the process startup to 5 h of test.

	$\ell_{(m)}$	Bi	ΔT (°C)
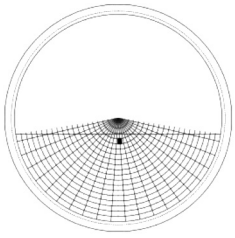	0.280	2.626	11.8
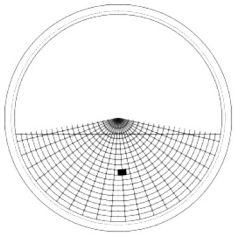	0.232	2.183	13.3
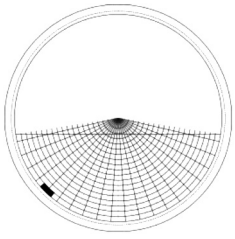	0.004	0.037	16.5

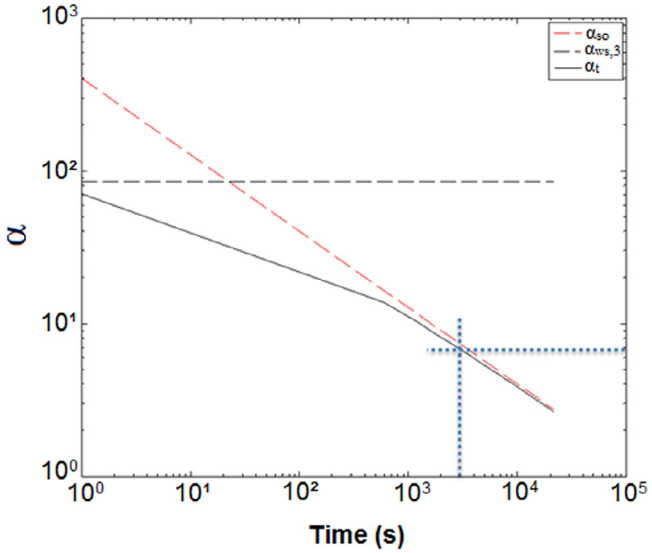

Fig. 13. Variation of the heat transfer coefficients along the process for the studied system. Experimental parameters correspond to the detail in the lower right corner. (Legend: Dashed, black: Heat transfer coefficient from wall to the first layer of particles including radiation; dashed red: penetration heat transfer coefficient; solid black: overall heat transfer coefficient).

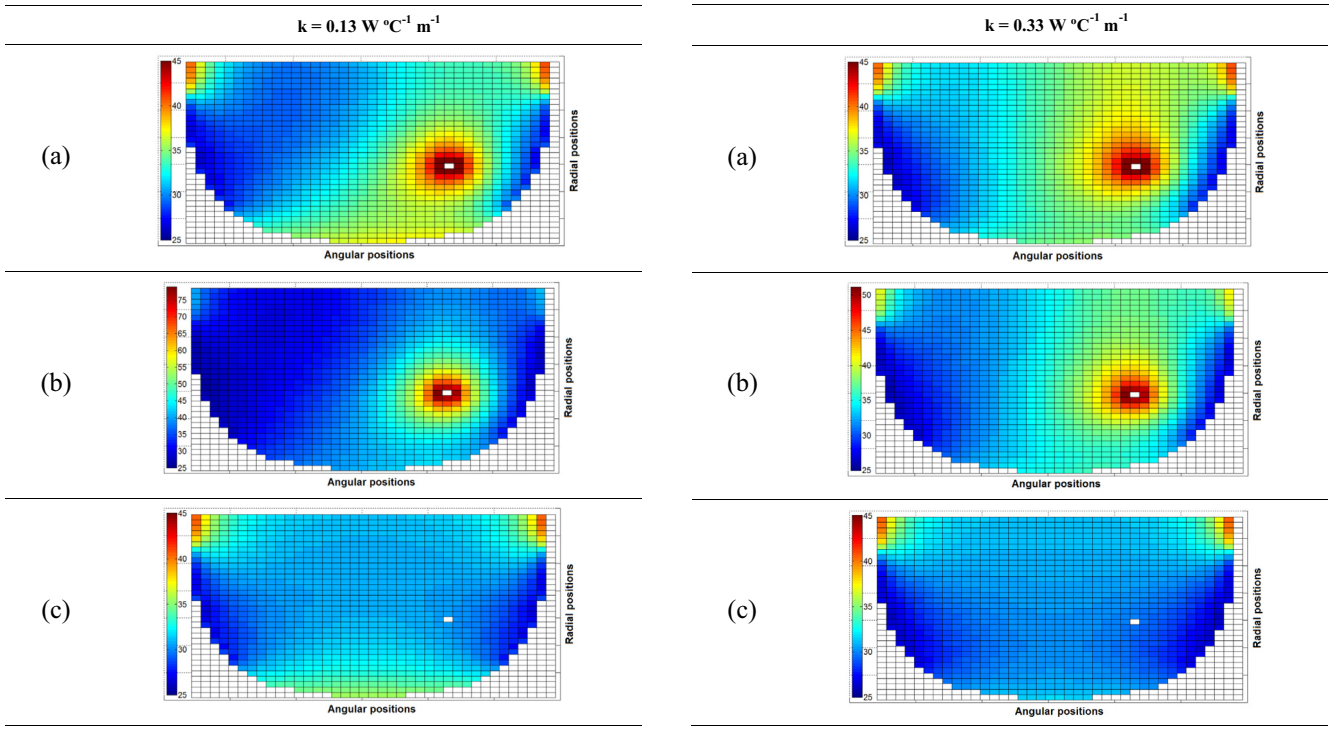

Fig. 14. Simulated temperature profiles predicted by the two-dimensional heat transfer model considering the heating element within the bed of particles, for the filling degree 0.4 and 10 h of simulation (h_w = 2.0 W °C^{-1} m^{-2}; h_s = 0.24 W °C^{-1} m^{-2}). Three options of including the heat element on the model has been used: (a) constant temperature at the interface bed-heat element; (b) constant flux at the interface bed-heat element; (c) a heat generation term in the heat balance.

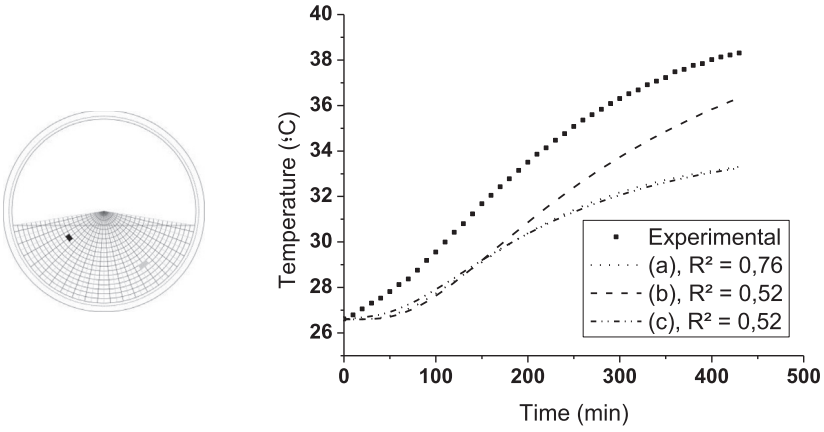

Fig. 15. Measured and calculated temperatures by two-dimensional model along time for the configuration with a heating element inserted within the bed for filling degree 0.4 (k = 0.32 W °C^{-1} m^{-1}; h_w = 3.0 W °C^{-1} m^{-2}; h_s = 0.24 W °C^{-1} m^{-2}). Three options of including the heating element on the model has been used: (a) constant temperature at the interface bed-heating element; (b) constant flux at the interface bed-heating element; (c) a heat generation term in the heat balance.

was similar to the experimental profile, although the calculated temperatures were always lower than the measured ones, as can be seen in Fig. 15. Hence, it was supposed that h_s should be higher than the adopted value. Since the alternative (b) presented the most promising results, the following simulations have been carried out only for this option.

Considering the possible influence of h_s on the simulated results and that no values are available in literature for h_s in a condition similar to the one here presented, the central composite design

Table 5
Range of parameters used to fit the calculated to the experimental temperatures for the situation with heating element within the bed. The parameters were applied to a CCD to optimize the search of the best fit.

Parameters	Ranges
h_s	1.8–2.4 W °C^{-1} m^{-2}
k	0,27–0.33 W °C^{-1} m^{-1}
h_w	1.2–3.0 W °C^{-1} m^{-2}

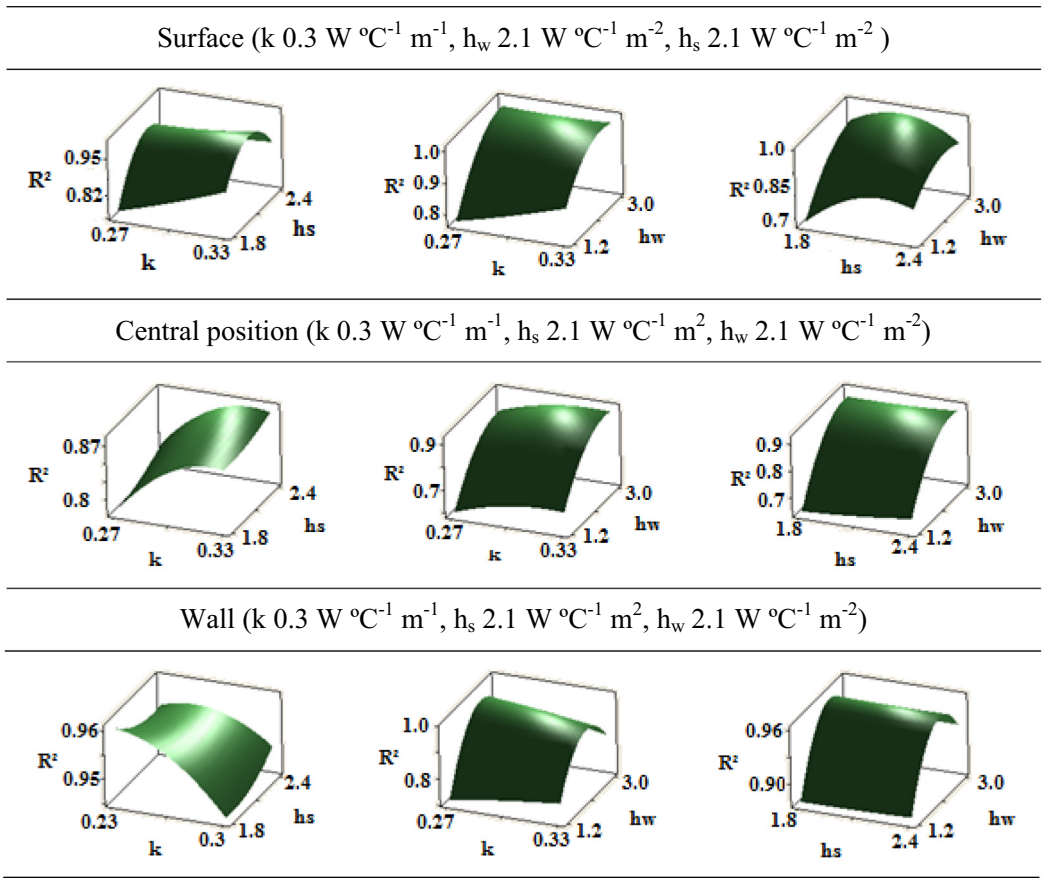

Fig. 16. Response surfaces generated by central composite design (CCD) used to estimation of parameters h_s, h_w and k for filling degree 0.4.

(CCD) was proposed considering the variation of the three parameters, as shown in Table 5. This range of parameters was obtained by previous CCD, beginning from range shown in Table 2. Fig. 16 shows the response surfaces for the determination coefficient for all combinations of parameters, where it can be observed that all surfaces are well represented by a quadratic model and that the optimum condition could be found. All the tested parameters have been considered significant by the ANOVA at 95% of confidence level, and the best set of parameters were $k = 0.33\ W\ °C^{-1}\ m^{-1}$, $h_w = 2.3\ W\ °C^{-1}\ m^{-2}$ and $h_s = 2.8\ W\ °C^{-1}\ m^{-2}$. A good agreement between the measured and the calculated temperatures can be observed in Fig. 17, except for the central region of the bed, dominated by the conduction mechanism. It must be pointed out that the physical property k is a spatially-varying and in the calculation procedure it has been assumed isotropic and constant. Probably, if two different contributions of k have been used, one for the radial direction and other for the angular direction, the results could be improved. Nevertheless, considering that the determination coefficient was high for all regions, the model can be considered satisfactory.

The best values of the fitting parameters were close to the ones presented for the configuration with air flowing through the headspace, except for the parameter h_s. The values of k and h_w are reasonable, since the mechanisms of heat transfer within the bed and in the boundary bed-drum wall did not change because of the insertion of the heating element. Nevertheless, the significant increase on the parameter h_s should be better understood, since the conventional free convection at the bed surface has been underestimated for the current problem.

3.7. Further studies towards a model to represent a solid-state fermentation bioreactor in partially filled horizontal stationary drums

As mentioned before, solid-state fermentation drum bioreactors often operate in stationary conditions and are rotated only in specific moments of the process (e.g. to homogenize the temperature and to replenish evaporated water). The biological process is quite complex, since the composition and physical-chemical properties of the organic particles change along the process. Besides, the microorganism, microscopically non-detectable at the early stages of the process, branches its hyphaes to the interparticle pores and its physical-chemical properties are quite different from the cultivation medium. Therefore, the porosity is expected to change during the fermentation, as well as the particle size and composition. Another important aspect in the SSF is that the water requirements of the microorganism are quite strict, and, due to the heat metabolically generated, mass transfer will certainly occur.

Therefore, the model here proposed is the first step to achieve a more complex model. The next step in this search should be the proposition of a mass transfer model for a stationary drum partially filled with hygroscopic particles, which would be coupled with the heat transfer model, now including the evaporative heat transfer term. Simultaneously, the porosity variation along the cultivation time should be obtained for the chosen microorganism and cultivation medium, as well as the shape and composition alterations of the solid phase. The possible modification of the physical properties of the porous medium (e.g. particle density, bulk bed density, effective thermal conductivity, and effective mass transfer diffusivity) due to the microbial growth should be

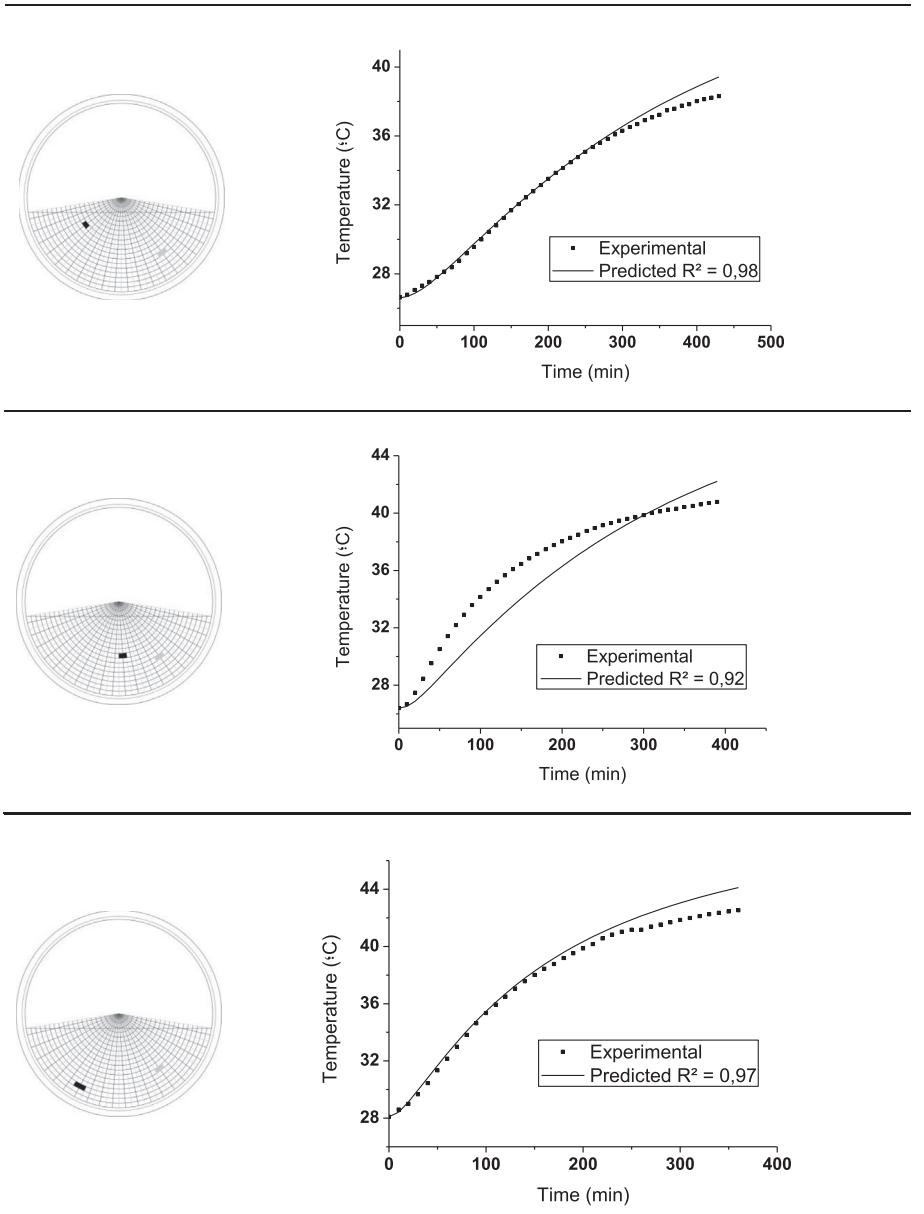

Fig. 17. Experimental temperature profiles for the configuration with a heating element inserted within the bed for the filling degree 0.4, and temperature profiles predicted by the two-dimensional model with a second kind boundary condition at the interface bed-heating element and a third kind boundary condition between the bed and the drum-wall ($k = 0.33\ W\ °C^{-1}\ m^{-1}$; $h_w = 2.3\ W\ °C^{-1}\ m^{-2}$; $h_s = 2.8\ W\ °C^{-1}\ m^{-2}$).

addressed. Finally, an accurate forecast of the microbial generated heat should be provided.

Hence, it is unwise the proposition of such complex model in a single step, and the proposition of individual models for each aspect of the fermentation process might be useful for other branches of the process engineering other than the SSF.

4. Conclusions

The heat transfer in a stationary horizontal drum partially filled with glass beads has been studied. A mathematical model has been proposed and the situations in which air flowed in the headspace and with an electrical heating element inserted within the bed were discussed. For air flowing in the headspace, the bed-to-air convective heat transfer coefficient (h_s) has been experimentally obtained and its value was close to the coefficient calculated assuming the bed as a flat plate with air flowing in parallel to it in laminar flow. For the situation in which the heat element was inserted within the bed, two boundary conditions were tested, assuming constant temperature and constant heat flux at the boundary, and a heat generation term has been included in the heat balance, and the best results were obtained with the constant flux boundary condition. Two boundary conditions have been applied to the model to represent the contact bed-to-drum wall, a constant wall temperature boundary condition and a convective boundary condition, and the latter proved to be more physically consistent. The parameters effective thermal conductivity (k) and wall-to-bed heat transfer coefficient (h_w) have been adjusted for both tested situations in order to provide the best fit between the temperatures forecasted by the model and the temperatures measured in several radial and angular positions along the time of process. The experiments have been carried out with glass beads with filling degrees 0.2 and 0.4, controlling the drum-wall

temperature, the air entrance temperature or the electrical heating element power. For the situation with the heating element, the parameter h_s was also adjusted. The adjusted value of k was amidst the values observed in literature for beds without flowing air, while the value of h_w was lower than the ones found in literature for air flowing perpendicularly to packed beds, indicating strong external heat transfer resistance. The best value of h_s was closer to the one experimentally obtained than to the one estimated by a natural convection correlation of air in contact to a hot flat plate. The results here obtained will be of value to simulate and operate solid-state drum bioreactors and other systems with high filling degrees.

Acknowledgements

The authors gratefully acknowledge the sponsors of this work: Coordination for the Improvement of Higher Education Personnel (CAPES), Fundação de Amparo à Pesquisa do Estado de São Paulo (FAPESP) (Processos #2011/07453-5, #2012/13939-0, #2014/25183-3, #2014/23453-3 and #2015/00362-5) and German Federal Ministry of Science and Education (BMBF), as part of the InnoProfile-Transfer project NaWiTec (Grant #03IPT701X).

References

[1] M.Z. Alam, A.A. Mamun, I.Y. Qudsieh, S.A. Muyibi, H.M. Salleh, N.M. Omar, Solid state bioconversion of oil palm empty fruit bunches for cellulase enzyme production using a rotary drum bioreactor, Biochem. Eng. J. 46 (2009) 61–64.
[2] L.M. Grajales, N.M. Xavier, J.P. Henrique, J.C. Thoméo, Mixing and motion of rice particles in a rotating drum, Powder Technol. 222 (2012) 167–175.
[3] Y.S. Lin, W.C. Lee, K.J. Duan, Y.H. Lin, Ethanol production by simultaneous saccharification and fermentation in rotary drum reactor using thermotolerant *Kluveromyces marxianus*, Appl. Energy 105 (2013) 389–394.
[4] B.K. Lonsane, N.P. Ghildyal, S. Budiatman, S.V. Ramakrishna, Engineering aspects of solid state fermentation, Enz. Microbiol. Technol. 7 (1985) 258–265.
[5] A. Pandey, Solid-state fermentation, Biochem. Eng. J. 13 (2003) 81–84.
[6] S. Bhargav, B.P. Panda, M. Ali, S. Javed, Solid-state fermentation: an overview, Chem. Biochem. Eng. 22 (2008) 49–70.
[7] R.R. Singhania, A.K. Patel, C.R. Soccol, A. Pandey, Recent advances in solid-state fermentation, Biochem. Eng. J. 44 (2009) 13–18.
[8] J. Cordova, M. Nemmaoui, M. Ismaili-Alaoui, A. Morin, S. Roussos, M. Raimbault, B. Benjilali, Lipase production by solid state fermentation of olive cake and sugar cane bagasse, J. Mol. Catal. B: Enzyme 5 (1998) 75–78.
[9] M. Stredansky, E. Conti, Xanthan production by solid state fermentation, Process Biochem. 34 (1999) 581–587.
[10] S. Miura, T. Arimura, N. Itoda, L. Dwiarti, J.B. Feng, C.H. Bin, M. Okabe, Production of L-latic acid from corncob, J. Biosci. Bioeng. 97 (2004) 153–157.
[11] D. Silva, K. Tokuioshi, E.S. Martins, R. Silva, E. Gomes, Production of pectinase by solid-state fermentation with *Penicillium viridicatum* RFC3, Process Biochem. 40 (2005) 2885–2889.
[12] H. Anto, U.B. Trivedi, K.C. Patel, Glucoamylase production by solid-state fermentation using rice flake manufacturing waste products as substrate, Bioresour. Technol. 97 (2006) 1161–1166.
[13] R. Paranthaman, K. Alagusundaram, J. Indhumanthi, Production of protease from rice mil wastes by *Aspergillus niger*in solid state fermentation, W. J. Agric. Sci. 5 (2009) 308–312.
[14] M.Y. Juan, C.C. Chou, Enhancement of antioxidant activity, total phenolic and flavonoid content of black soybeans by solid state fermentation with *Bacillus subtilis* BCRC 14715, Food Microbiol. 27 (2010) 586–591.
[15] N. Bansal, R. Tewari, R. Soni, S.K. Soni, Production of cellulases from *Aspergillus niger* NS-2 in solid state fermentation on agricultural and kitchen waste residues, Waste Managem. 32 (2012) 1341–1346.
[16] A.I. Zanelato, V.M. Shiota, E. Gomes, R. Silva, J.C. Thoméo, Endoglucanase production with the newly isolated *Myceliophtora sp.* i-1d3b in a packed bed solid state fermentor, Braz. J. Microbiol. 43 (2012) 1536–1544.
[17] A. Biz, A.T.J. Finkler, L.O. Pitol, B.S. Medina, N. Krieger, D.A. Mitchell, Production of pectinases by solid-state fermentation of a mixture of citrus waste and sugarcane bagasse in a pilot-scale packed-bed bioreactor, Biochem. Eng. J. 111 (2016) 54–62.
[18] D.A. Mitchell, N. Krieger, D.M. Stuart, A. Pandey, New developments in solid-state fermentation: II. Rational approaches to the design, operation and scale-up of bioreactors, Process Biochem. 35 (2000) 1211–1225.
[19] E.Q. Wang, S.Z. Li, L. Tao, X. Geng, T.C. Li, Modeling of rotating drum bioreactor for anaerobic solid-state fermentation, Appl. Energy. 87 (2010) 2839–2845.
[20] M. A. I. Schutyser, W. J. Briels, R. M. Boom, A. Rinzema, Combined discrete particle and continuum model predicting solid-state fermentation in a drum fermentor, Wiley, Intersci. 86 (2004) 405-413.
[21] G. Saucedo-Castañeda, M. Gutiérrez-Rojas, G. Bacquet, M. Raimbault, G. Viniegra-González, Heat transfer simulation in solid substrate fermentation, Biotechnol. Bioeng. 35 (1990) 802–808.
[22] P. Sangsurasak, D.A. Mitchell, The investigation of transient multidimensional heat transfer in solid state fermentation, Chem. Eng. J. 60 (1995) 199–204.
[23] P. Sangsurasak, D.A. Mitchell, Validation of a model describing two-dimensional heat transfer during solid-state fermentation in a packed bed bioreactors, Biotechnol. Bioeng. 60 (1998) 739–749.
[24] D.A. Mitchell, A. Pandey, P. Sangsurasak, N. Krieger, Scale-up strategies for packed-bed bioreactors for solid-state fermentation, Process Biochem. 35 (1999) 167–178.
[25] M.A. Fanaei, B.M. Vaziri, Modeling of temperature gradients in packed-bed solid-state bioreactors, Chem. Eng. Process. 48 (2009) 446–451.
[26] F.P. Casciatori, A. Bück, J.C. Thoméo, E. Tsotsas, Two-phase and two-dimensional model describing heat and water transfer during solid-state fermentation within a packed-bed bioreactor, Chem. Eng. J. 287 (2016) 103–116.
[27] A.A. Boateng, P.V. Barr, A thermal model for the rotary kiln including heat transfer within the bed, Int. J. Heat Mass Transfer. 39 (1996) 2131–2147.
[28] Y.L. Ding, J.P.K. Seville, R. Forster, D.J. Parker, Solids motion in rolling mode rotating drums operated at low to medium rotational speeds, Chem. Eng. Sci. 56 (2001) 1769–1780.
[29] F. Herz, L. Mitov, E. Specht, R. Stanev, Experimental study of the contact heat transfer coefficient between the covered wall and solid bed in rotary drums, Chem. Eng. Sci. 82 (2012) 312–318.
[30] A.I. Nafsun, F. Herz, Experiments on the temperature distribution in the solid bed of rotary drums, Appl. Thermal Eng. 103 (2016) 1039–1047.
[31] L.M. Grajales, Development of a rotary drum bioreactor for cellulolytic enzymes production by solid-state fermentation (Ph.D. Thesis), PPG-ECA/UNESP, São José do Rio Preto, 2014, In Protuguese.
[32] S. Whitaker, Forced convection heat transfer correlations for flow in pipes, past flat plates, single cylinders, single spheres, and for flow in packed beds and tube bundles, AIChE J. 18 (1972) 361–371.
[33] O. Aydin, L. Guessous, Fundamental correlations for laminar and turbulent free convection from a uniformly heated vertical plate, Int. J. Heat Mass Transfer. 44 (2001) 4605–4611.
[34] A. Pantokratoras, Laminar free-convection in water with variable physical properties adjacent to a vertical plate with uniform heat flux, Int. J. Heat Mass Transfer 46 (2003) 725–729.
[35] W. Kast, H. Klan, Heat Transfer by Free Convection: External Flows, Springer Verlag, Berlin, VDI Heat Atlas, 2010.
[36] C.A. Coberly, W.R. Marshall, Temperature gradients in gas stream flowing through fixed granular beds, Chem. Eng. Prog. 47 (1951) 141–150.
[37] J.J. Lerou, G.F. Froment, Estimation of heat transfer parameters in packed beds from radial temperature profiles, Chem. Eng. J. 15 (1978) 233–237.
[38] J.C. Thoméo, J.T. Freire, Heat transfer in fixed bed: a model non-linearity approach, Chem. Eng. Sci. 55 (2000) 2329–2338.
[39] E. Tsotsas, E.U. Schlünder, Heat transfer in packed beds with fluid flow: remarks on the meaning and the calculation of a heat transfer coefficient at the wall, Chem. Eng. Sci. 45 (1990) 819–837.
[40] D.M. Himmelblau, Basic Principles and Calculations in Chemical Engineering, Prentice-Hall, Englewood Cliffs, 1982.
[41] R.H. Perry, C.H. Chilton, Chemical Engineer's Handbook, McGraw-Hill, 1973.
[42] M.N. Abbas, Modeling of porosity equation for water flow through packed bed of monosize spherical packing, J. Eng. Dev. 15 (2011) 205–226.
[43] S. Masamune, J.M. Smith, Thermal conductivity of beds of spherical particles, Ind. Eng. Chem. Fund. 2 (1963) 136–143.
[44] A. De Wash, G. Froment, Heat transfer in packed bed, Chem. Eng. Sci. 27 (1972).
[45] M. Kent, K. Christiansen, I.A. van Haneghem, E. Holtz, M.J. Morley, P. Nesvadba, K.P. Paulsen, Collaborative measurements of thermal properties of foods, J. Food Eng. 3 (1984) 117–150.
[46] E.U. Sclünder, N. Mollekopf, Vacuum contact drying of free slowing mechanically agitated particulate material, Chem. Eng. Process. 18 (1984) 93–111.
[47] E. Tsotsas, E.U. Schlünder, Contact drying of mechanically agitated particulate material in the presence of inert gas, Chem. Eng. Process. 20 (1986) 277–285.